Inorganic Chemistry

Article

pubs.acs.org/IC

Mercury Bismuth Chalcohalides, $Hg_3Q_2Bi_2Cl_8$ (Q = S, Se, Te): Syntheses, Crystal Structures, Band Structures, and Optical Properties

Arief C. Wibowo,[†] Christos D. Malliakas,[†,‡] Duck Young Chung,[†] Jino Im,[§] Arthur J. Freeman,[§] and Mercouri G. Kanatzidis*[,†,‡]

[†]Materials Science Division, Argonne National Laboratory, Argonne, Illinois 60439, United States

[‡]Department of Chemistry and [§]Department of Physics and Astronomy, Northwestern University, Evanston, Illinois 60208, United States

Supporting Information

ABSTRACT: Three quaternary mercury bismuth chalcohalides, $Hg_3Q_2Bi_2Cl_8$ (Q = S, Se, Te), are reported along with their syntheses, crystal structures, electronic band structures, and optical properties. The compounds are structurally similar with a layer comprised of a hole perforated sheet network of $[Hg_3Q_2]^{2+}$ (Q = S and Te) that forms by fused cyclohexane, chairlike Hg_6Q_6 rings. The cationic charge in the network is balanced by edge-sharing monocapped trigonal-prismatic anions of $[Bi_2Cl_8]^{2-}$ that form a two-dimensional network located between layers. Compound **1**, $Hg_3S_2Bi_2Cl_8$, crystallizes in the monoclinic space group $C12/m1$ with a = 12.9381(9) Å, b = 7.3828(6) Å, c = 9.2606(6) Å, and β = 116.641(5)°. Compound **2**, $Hg_3Te_2Bi_2Cl_8$, crystallizes in the monoclinic space group $C12/c1$ with a = 17.483(4) Å, b = 7.684(2) Å, c = 13.415(3) Å, and β = 104.72(3)°. The crystals of the $Hg_3Se_2Bi_2Cl_8$ analogue exhibit complex modulations and structural disorder, which complicated its structural refinement. Compounds **1** and **2** melt incongruently and show band gaps of 3.26 and 2.80 eV, respectively, which are in a good agreement with those from band-structure density functional theory calculations.

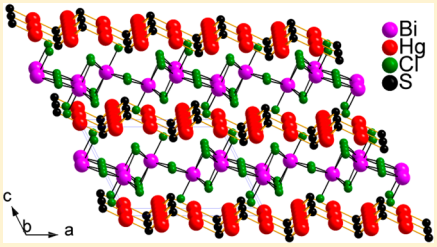

INTRODUCTION

Ternary metal chalcohalides are hybrid materials whose compositions lie between those of binary chalcogenides and binary halides.[1] Given the same elements, the energy band gaps of the metal chalcohalides lie between those of binary chalcogenides and binary halides. The former generally have significantly lower energy gaps than the latter, while the ternary metal chalcohalides have intermediate band gaps, as illustrated previously.[2] Different potential applications have been reported for hybrid chalcohalides such as X-ray and γ-ray detectors,[2] nonlinear optics,[3] phase transitions,[4] and upconversion luminescence.[5] We are interested in exploring highly dense, heavy-element-containing chalcohalides, such as mercury and bismuth, as part of our search to identify potential candidates for X-ray and γ-ray semiconductor detectors. Both mercury(II) and bismuth(III) not only adopt closed-shell electronic configurations but also have large ionic radii with flexible coordination environments, giving rise to interesting molecular architectures.[6] Recent reports on quaternary mercury-based chalcohalides include $[Hg_3Te_2][UCl_6]$,[7] $[Hg_3Q_2][MX_6]$ (Q = S, Se; M = Zr, Hf; X = Cl, Br),[8] Hg_3AsQ_4X (Q = S, Se; X = Cl, Br, I),[9] $Hg_3ZnS_2Cl_4$,[10] $[Hg_8As_4][Bi_3Cl_{13}]$,[11] $(Hg_2Cd_2S_2Br)Br$,[12] and $Hg_7InS_6Cl_5$.[13] Herein, we report two mercury bismuth chalcohalides, $Hg_3S_2Bi_2Cl_8$ (**1**) and $Hg_3Te_2Bi_2Cl_8$ (**2**), along with their syntheses, structural characterizations, electronic-band-structure calculations, and optical properties. The $Hg_3Se_2Bi_2Cl_8$ (**3**) analogue was also synthesized, but because of structural modulations and disorder, structural refinement was not carried out.

EXPERIMENTAL SECTION

Chemicals in this work were used without further purification: $BiCl_3$ (99.9% metal basis, Alfa Aesar), $HgCl_2$ (99.9995% metal basis, Alfa Aesar) ,elemental mercury (99.999%, electronic grade, Sigma-Aldrich), sulfur chunks (99.999%, Spectrum Chemical Mfg. Corp.), selenium shots (99.999%, Plasmaterials), and tellurium shots (99.999%, Plasmaterials). All manipulations were done inside a nitrogen-filled glovebox.

Synthesis of HgQ (Q = S, Se, and Te). HgS was prepared by pipetting a stoichiometric amount of liquid mercury into a 15 mm o.d. × 12 mm i.d. fused-silica tube and then adding a stoichiometric amount of ground sulfur. The tube was flame-sealed under dynamic vacuum of ~10^{-4} mbar and then put into a programmable furnace. The furnace was heated to 400 °C over 12 h and held isothermally for 1 day, followed by cooling slowly to 50 °C over 6 h. The obtained ingot was ground to powder before use. The purity of the product was checked by powder X-ray diffraction (PXRD). A similar preparation procedure was adopted for HgSe and HgTe, but the furnace was heated to 550 °C over 16 h, held isothermally for 1 day, and then cooled slowly to 50 °C over 6 h. ***Caution!*** *Handling of mercury should be carried out in a fume hood or a glovebox, and the temperature was raised slowly to ensure that liquid mercury reacts without evaporating.*

Received: October 31, 2012

   dx.doi.org/10.1021/ic3023826 | *Inorg. Chem.* XXXX, XXX, XXX−XXX

Synthesis of $Hg_3S_2Bi_2Cl_8$ (1). Several attempts were made to obtain a quantitative yield of **1** using a stoichiometric mixture of HgS, $HgCl_2$, and $BiCl_3$ by (a) melting and slow cooling, (b) melting and quenching in air and ice water, (c) flame melting and ice water quenching, and (d) low-temperature annealing at 300 °C for solid-state diffusion. All of these conditions produced a mixture of **1** as the major product and impurities of ternaries (BiSCl and β-$Hg_3S_2Cl_2$). A quantitative yield of **1** was obtained after the addition of an excess of $BiCl_3$ (3-fold excess over what is required for a stoichiometric reaction) using the following conditions. A mixture of HgS (2 mmol), $HgCl_2$ (1 mmol), and $BiCl_3$ (6 mmol) was loaded into a 12 mm o.d. × 10 mm i.d. fused-silica tube. Then the tube was flame-sealed under vacuum (~10^{-4} mbar), put inside a programmable box furnace, heated to 300 °C over 24 h, and held isothermally for 12 h, followed by a shutdown of the furnace. The excess of $BiCl_3$ was washed away using methanol. A white polycrystalline powder with a slight pale-purple tint was obtained and amounted to a quantitative yield of **1**.

In the course of these experiments, we found that reaction with a 1:1 mixture of HgS and $BiCl_3$ provided single crystals of **1** suitable for structural characterization. This was done as follows. The thoroughly mixed powders of HgS and $BiCl_3$ at a 1:1 ratio were loaded into a 12 mm o.d. × 10 mm i.d. fused-silica tube. The tube was flame-sealed under vacuum (~10^{-4} mbar) and put inside a programmable furnace. The furnace was heated to 450 °C over 12 h and held isothermally for 1 day, followed by cooling slowly to 200 °C over 36 h and then to room temperature within 1 h. White, platelike crystals (~30% yield based on HgS) were obtained. The presence of mercury, bismuth, sulfur, and chlorine in the platelike crystals obtained was confirmed by scanning electron microscopy−energy-dispersive spectrometry (SEM−EDS).

Synthesis of $Hg_3Te_2Bi_2Cl_8$ (2). Unlike the sulfur analogue, a stoichiometric reaction of HgTe, $HgCl_2$, and $BiCl_3$ was successfully performed by solid-state diffusion at 200 °C to give a quantitative yield of **2**. A mixture of HgTe, $HgCl_2$, and $BiCl_3$ at a stoichiometric ratio was loaded into a 12 mm o.d. × 10 mm i.d. fused-silica tube. Then the tube was flame-sealed under vacuum (~10^{-4} mbar), put inside a programmable box furnace, heated to 200 °C over 14 h, and held isothermally for 48 h, followed by a shutdown of the furnace. Dark-green polycrystalline powder was obtained with a quantitative yield of **2**.

Single crystals of **2** suitable for structural characterization were prepared by a reaction of HgTe and $BiCl_3$ at a 1:1 ratio. The mixture in a sealed quartz tube was heated to 600 °C over 16 h and held isothermally for 24 h, followed by cooling slowly to 200 °C over 36 h and then to room temperature within 1 h. Greenish, platelike crystals were obtained at ~30% yield based on HgTe. The composition of the crystals was confirmed by SEM-EDS.

Synthesis of $Hg_3Se_2Bi_2Cl_8$ (3). The crystals were synthesized analogously to compound **2**. A ground 1:1 mixture of HgSe and $BiCl_3$ was sealed under vacuum (~10^{-4} mbar) in a 12 mm o.d. × 10 mm i.d. fused silica tube, heated to 600 °C over 16 h, and held isothermally for 24 h, followed by cooling slowly to 200 °C over 36 h and then to room temperature within 1 h. Orange, platelike crystals (~30% yield based on HgSe) were obtained. The presence of mercury, bismuth, selenium, and chlorine in the platelike crystals was confirmed by SEM-EDS. These crystals were further examined by single-crystal X-ray diffraction (XRD) and PXRD.

Single-Crystal XRD. Single-crystal XRD data were collected at 293 K on a STOE 2T image-plate diffractometer with Mo Kα radiation (λ = 0.71073 Å). An analytical absorption correction was applied to the data using the program *X-Red* on an optimized shape obtained with the aid of *X-Shape* software. The structures were solved by direct methods and refined with the *SHELXTL* software package. Thermal displacement parameters were anisotropically refined for all atomic positions. Data were collected on several single crystals, to check for consistency in the lattice parameters. The complete data collection parameters and details of the structure solution and refinement for the compounds are given in Table 1. The fractional coordinates, thermal displacement parameters (U_{eq}), and occupancies of all atoms with estimated standard deviations are given in Tables 2 and S1 in the Supporting Information, SI. The selected bond lengths and angles are given in Tables 3 and 4 for compounds **1** and **2**, respectively.

Table 1. Crystal Data and Structural Refinement of Compounds 1 and 2[a]

	1	2
empirical formula	$Hg_3S_2Bi_2Cl_8$	$Hg_3Te_2Bi_2Cl_8$
fw	1367.45	1558.53
temperature (K)	293(2)	293(2)
wavelength (Å)	0.71073	0.71073
cryst syst	monoclinic	monoclinic
space group	*C*12/*m*1	*C*12/*c*1
unit cell dimens		
a (Å)	12.9381(9)	17.483(4)
b (Å)	7.3828(6)	7.684(2)
c (Å)	9.2606(6)	13.415(3)
α (deg)	90.00	90.00
β (deg)	116.641(5)	104.72(3)
γ (deg)	90.00	90.00
volume (Å^3)	790.6(1)	1743.0(6)
Z	2	4
density (calcd) (g/cm^3)	5.744	5.939
abs coeff (mm^{-1})	52.789	50.933
F(000)	1148	2584
cryst size (mm^3)	0.1 × 0.03 × 0.06	0.1 × 0.03 × 0.07
θ range for data collection (deg)	4.55−34.87	3.16−24.99
index ranges	$-20 \le h \le +20$, $-11 \le k \le +11$, $-14 \le l \le +14$	$-20 \le h \le +20$, $-9 \le k \le +9$, $-15 \le l \le +15$
reflns collected	4685	5440
indep reflns	1706 [R_{int} = 0.0526]	1531 [R_{int} = 0.0914]
completeness to θ = 32.49° (%)	93.1	99.4
refinement method	full-matrix least squares on F^2	full-matrix least squares on F^2
data/restraints/param	1706/0/44	1531/0/71
GOF	1.038	0.946
final *R* indices [$I > 2\sigma(I)$]	$R1_{obs}$ = 0.0299, $wR2_{obs}$ = 0.0695	$R1_{obs}$ = 0.0304, $wR2_{obs}$ = 0.0690
R indices (all data)	$R1_{all}$ = 0.0366, $wR2_{all}$ = 0.0717	$R1_{all}$ = 0.0373, $wR2_{all}$ = 0.0716
extinction coeff	0.00088(9)	0.00034(3)
largest diff peak and hole (e/Å^3)	3.728 and −2.141	2.711 and −1.690

[a] $R1 = \sum||F_o| - |F_c||/\sum|F_o|$. $wR2 = \{\sum[w(F_o^2 - F_c^2)^2]/\sum[w(F_o^2)^2]\}^{1/2}$.

PXRD. Ground powder of the sample was used to collect PXRD patterns using a PanAlytical X'Pert Pro powder diffractometer (Cu Kα radiation λ = 1.5418 Å) over the 2θ range of 10−70°, with a step size of 0.02° and a scan speed of 0.25°/min.

UV−Vis Spectroscopy. Optical diffuse-reflectance measurements were performed at room temperature using a Shimadzu UV-3600 spectrophotometer operating in the 200−2500 nm region. The instrument was equipped with an integrating sphere and controlled by a personal computer. $BaSO_4$ was used as a 100% reflectance standard. The sample was prepared by grinding the powder and spreading it on a compacted surface of the powdered standard material, preloaded into a sample holder. The reflectance versus wavelength data generated were used to estimate the band gap of the material by converting reflectance to absorption data according to the Kubelka−Munk equation $\alpha/S = (1 - R)^2/2R$, where R is the reflectance and α and S are the absorption and scattering coefficients, respectively.[14]

Differential Thermal Analysis (DTA). Experiments were performed on a Shimadzu DTA-50 thermal analyzer. A sample (~30 mg) of ground crystalline material was sealed in a silica ampule under

dx.doi.org/10.1021/ic3023826 | *Inorg. Chem.* XXXX, XXX, XXX−XXX

Table 2. Atomic Coordinates (×10^4) and Equivalent Isotropic Displacement Parameters (Å^2 × 10^3) at 293(2) K with Estimated Standard Deviations in Parentheses

label	x	y	z	occupancy	U_{eq} [a]
		(a) $Hg_3S_2Bi_2Cl_8$			
Bi(1)	1271(1)	0	4262(1)	1	17(1)
Hg(1)	2500	2500	0	1	25(1)
Hg(3)	0	5000	0	1	27(1)
Cl(1)	0	−2438(3)	5000	1	28(1)
Cl(2)	1930(2)	2669(2)	2870(2)	1	27(1)
Cl(3)	−492(2)	0	1494(3)	1	32(1)
S(1)	1249(2)	5000	−1249(2)	1	19(1)
		(b) $Hg_3Te_2Bi_2Cl_8$			
Bi(1)	409(1)	2321(1)	9374(1)	1	24(1)
Hg(1)	2500	7500	10000	1	42(1)
Hg(2)	2533(1)	5145(1)	7432(1)	1	47(1)
Te(1)	1666(1)	7511(1)	8059(1)	1	32(1)
Cl(1)	1040(2)	5241(4)	10366(2)	1	36(1)
Cl(2)	1032(2)	2702(4)	7758(2)	1	39(1)
Cl(3)	1744(2)	1076(4)	10244(2)	1	40(1)
Cl(4)	10(2)	1089(4)	11134(2)	1	35(1)

[a] U_{eq} is defined as one-third of the trace of the orthogonalized U_{ij} tensor.

Table 3. Representative Bond Lengths (Å) and Bond Angles (deg) of 1[a]

Hg(1)−S(1)	2.385(1)
Hg(1)−S(1)	2.385(1)
Hg(3)−S(1)	2.372(2)
Hg(3)−S(1)	2.372(2)
Hg(3)−S(1)−Hg(1)	103.07(6)
Hg(3)−S(1)−Hg(1)	103.07(6)
Hg(1)−S(1)−Hg(1)	101.43(6)
Bi(1)−Cl(3)	2.556(2)
Bi(1)−Cl(2)	2.694(2)
Bi(1)−Cl(2)	2.694(2)
Bi(1)−Cl(1)	2.724(1)
Bi(1)−Cl(1)	2.724(1)

[a] Symmetry transformations used to generate equivalent atoms: (1) $x, -y, z$; (2) $-x, -y, -z + 1$; (3) $-x + {}^1/_2, -y + {}^1/_2, -z$; (4) $x + {}^1/_2, y + {}^1/_2, z$; (5) $-x, -y, -z$; (6) $-x, -y + 1, -z$; (7) $x - {}^1/_2, y - {}^1/_2, z$; (8) $-x, y, -z$; (9) $-x + {}^1/_2, y + {}^1/_2, -z$.

Table 4. Representative Bond Lengths (Å) and Bond Angles (deg) of 2[a]

Hg(1)−Te(1)	2.642(1)
Hg(1)−Te(1)	2.642(1)
Hg(2)−Te(1)	2.6377(9)
Hg(2)−Te(1)	2.6388(9)
Te(1)−Hg(2)	2.6377(9)
Hg(2)−Te(1)−Hg(2)	93.70(3)
Hg(2)−Te(1)−Hg(1)	93.05(3)
Hg(2)−Te(1)−Hg(1)	95.40(3)
Bi(1)−Cl(3)	2.519(3)
Bi(1)−Cl(2)	2.678(2)
Bi(1)−Cl(1)	2.697(3)
Bi(1)−Cl(4)	2.759(3)
Bi(1)−Cl(4)	2.792(2)

[a] Symmetry transformations used to generate equivalent atoms: (1) $-x, -y, -z + 2$; (2) $-x + {}^1/_2, -y + {}^3/_2, -z + 2$; (3) $-x + {}^1/_2, y - {}^1/_2, -z + {}^3/_2$; (4) $-x + {}^1/_2, y + {}^1/_2, -z + {}^3/_2$.

vacuum. A similar ampule of equal mass filled with Al_2O_3 was sealed and placed on the reference side of the detector. The sample was heated to 400 °C (compound **1**) or to 450 °C (compound **2**) at 5 °C/min, and after 10 min, it was cooled at a rate of −5 °C/min to 50 °C. Two cycles of heating and cooling were applied to the samples. The residues of the DTA experiments were examined by PXRD.

Band-Structure Calculations. To investigate the electronic structures of both compounds, first-principles calculations were performed within the density functional theory (DFT) formalism using the full potential linearized augmented plane wave method.[15] The muffin tin radii for mercury, bismuth, chlorine, sulfur, and tellurium were chosen to be 2.40, 2.60, 1.90, 2.00, and 2.20 Bohr, respectively, and the energy cutoffs for the plane-wave basis and star functions were set to 16 and 100 Ryd, respectively. For *k*-point sampling, 8 × 10 × 8 and 6 × 6 × 4 regular meshes were chosen for compounds **1** and **2**, respectively. Within the local density approximation (LDA), the Hedin−Lundqvist form[16] was employed for the exchange-correlation functional and spin−orbit coupling (SOC) was treated by a second variation method.[17] For a better evaluation of the band gap, which is usually underestimated in LDA formalism, we employed the nonlocal scheme of the screened-exchange LDA (sX-LDA) method,[18] which leads to a good agreement with experimentally measured band gaps as well as band topology.[19]

RESULTS AND DISCUSSION

Synthesis. The reactions of mercury chalcogenides with mercury dichloride and bismuth trichloride in a closed ampule under relatively low temperatures (200−300 °C) yield a series of air-stable, isotypic compounds of the general formula $Hg_3Q_2Bi_2Cl_8$ (Q = S, Se, and Te). Synthesizing a single phase of **1** is challenging. In order to obtain a quantitative yield of **1**, we attempted several reactions using a stoichiometric mixture of HgS, $HgCl_2$, and $BiCl_3$. These reactions involved a variety of heat treatments such as (a) melting and slow cooling, (b) melting and quenching in air and ice water, (c) flame melting and ice water quenching, and (d) low-temperature annealing at 300 °C for solid state diffusion. None of these synthetic attempts were successful in giving single-phase samples of **1**, and the ternaries BiSCl and β-$Hg_3S_2Cl_2$ were always present as minor products.

A quantitative yield was finally obtained after the addition of about a 3-fold excess of $BiCl_3$ and running of the reaction at

dx.doi.org/10.1021/ic3023826 | Inorg. Chem. XXXX, XXX, XXX−XXX

300 °C. The PXRD pattern of the product obtained is shown in Figure 1. The excess of $BiCl_3$ suppresses the formation of BiSCl

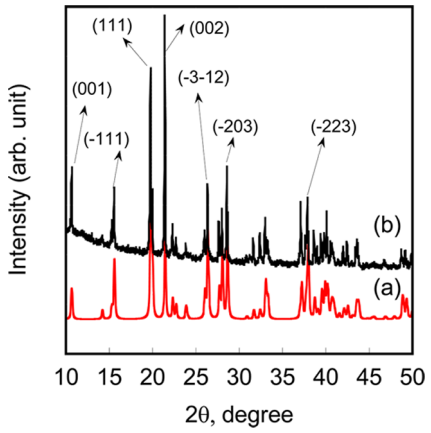

Figure 1. PXRD patterns of compound **1**: (a) simulated; (b) observed.

and β-$Hg_3S_2Cl_2$ phases. We also observed that an extended period of heating **1** at temperatures between 350 and 450 °C led to the formation of β-$Hg_3S_2Cl_2$ and $BiCl_3$ as separate major entities, suggesting incongruent melting.

Unlike **1**, the synthesis of **2** is less complicated. A quantitative yield of a dark-green polycrystalline powder of **2** was obtained using a stoichiometric ratio of HgTe, $HgCl_2$, and $BiCl_3$ by a low-temperature route at 200 °C, as shown in the PXRD pattern of the product obtained (Figure 2). **2** also melts incongruently, which is a common behavior in mercury chalcohalides.[8,13]

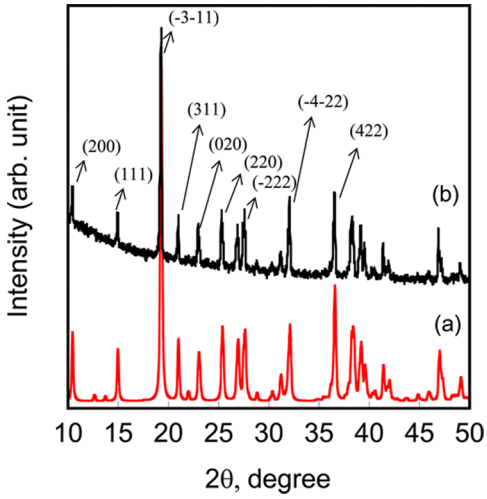

Figure 2. PXRD patterns of compound **2**: (a) simulated; (b) observed.

Preparing good-quality single crystals of **3** was difficult, and stoichiometric reactions did not produce large crystals suitable for single-crystal XRD. Such crystals could be obtained only at ~30% yield from the 1:1 reaction of HgSe and $BiCl_3$ at 600 °C. The obtained average unit cell parameters are a = 6.971(1) Å, b = 8.634(2) Å, c = 8.120(2) Å, and β = 106.87(3)°. Because of modulation and structural disorder observed in the structural model, it was difficult to obtain an acceptable structural refinement for this compound. The structural refinements as well as PXRD patterns, however, show that **3** probably has a structure related to those of the other two analogues.

Investigations aimed at synthesizing other quaternary chalcohalide analogues using HgQ (Q = S, Se, Te) with different halides, BiX_3 (X = Br, I) or SbX_3 (X = Cl, Br, I), under conditions similar to those described above were unsuccessful, yielding the ternaries $Hg_3Q_2X_2$ and BiQX or SbQX and BiX_3 or SbX_3.

Structural Description. Compounds **1** and **2** have structures similar to those of $Hg_3Te_2UCl_6$[7] and $Hg_3Q_2MX_6$ (Q = S, Se; M = Zr, Hf; X = Cl, Br),[8] which are composed of $[Hg_3Q_2]^{2+}$ (Q = S, Te) layers that form from fused Hg_6Q_6 rings having a cyclohexane chair-type conformation. A two-dimensional (2D) network of bismuth halide counteranions is intercalated between the $[Hg_3Q_2]^{2+}$ interlayer, as shown in Figures 3 and S2 in the SI. As shown in Figure 4, compounds **1**

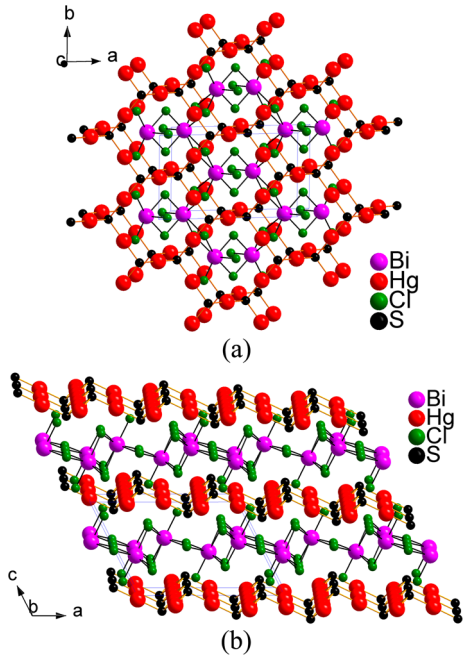

Figure 3. Overall 2D structure of compound **1** viewed along crystallographic (a) c and (b) b axes.

and **2** have dinuclear metal halides (Bi_2Cl_8) instead of mononuclear metal halides as observed in $Hg_3Te_2UCl_6$ and $Hg_3Q_2MX_6$ (Q = S, Se; M = Zr, Hf; X = Cl, Br).[7,8] This leads to the resulting formula $Hg_3Q_2Bi_2Cl_8$ (Q = S, Se, Te), with a correspondingly larger cell volume.

The mercury atoms are two-coordinated with a linear geometry. The chalcogen atoms are three-coordinated, QHg_3, forming trigonal pyramids. The Hg_6S_6 chair conformation is distorted in compound **1**, as indicated by its interior bond angles and bond lengths, shown in Table 3. Normal cyclohexane with a chair conformation has interior bond angles of 109.5° with similar C−C bond distances. In compound **1**, the interior bond angles (Hg−S−Hg) are less than 109.5° [ranging from 101.43(8) to 103.07(6)°] and the interior bond distances (Hg−S) range from 2.372(2) to 2.385(1) Å. A more distorted chair conformation of Hg_6Te_6 is observed for compound **2**, shown in Table 4, in which the interior bond angles are even smaller [ranging from 93.05(3) to 95.40(3)°], with larger interior bond distances ranging from 2.6377(9) to 2.642(1) Å.

The bismuth atoms are seven-coordinated, forming monocapped trigonal prisms (Figure S3 in the SI) that edge share to

dx.doi.org/10.1021/ic3023826 | Inorg. Chem. XXXX, XXX, XXX−XXX

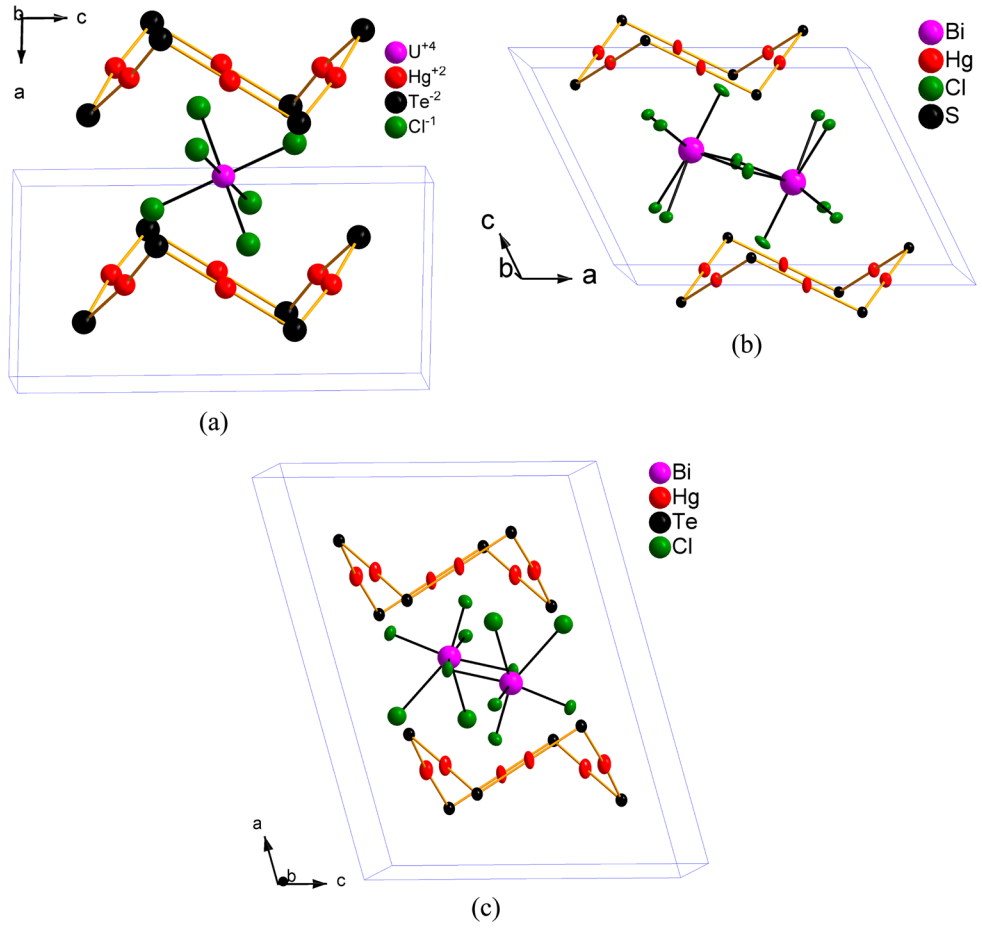

Figure 4. Structural comparison of (a) the previously reported $Hg_3Te_2UCl_6$,[7] (b) compound **1** with its thermal ellipsoid, and (c) compound **2** with its thermal ellipsoid.

form readily recognizable dimeric units that form 2D sheets along the crystallographic *ab* and *bc* planes for compounds **1** (Figure 5) and **2** (Figure 6), respectively. The sheets of Bi_2Cl_8

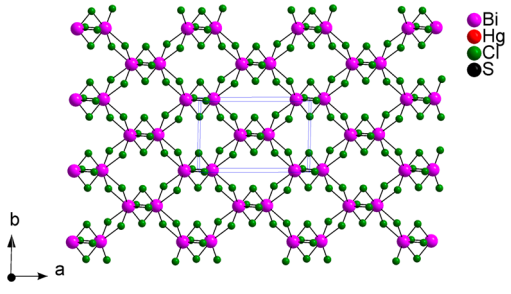

Figure 5. 2D network formation of Bi_2Cl_8 of compound **1** (viewed along the *c* axis), showing the formation of edge-sharing monocapped trigonal prisms. See the text for details.

in compound **1** possess a crystallographic 2-fold axis and a mirror plane that contains all bismuth atoms consistent with the space group *C*12/*m*1; see Figure 5. For compound **2**, the sheets of Bi_2Cl_8 possess a crystallographic 2-fold axis and a perpendicular *c*-glide plane; see Figure 6. Thus, the two sheets of Bi_2Cl_8 are very different in the two compounds.

Thermal Properties. The thermal behavior of compounds **1** and **2** was investigated by two consecutive cycles of heating and cooling using DTA measurements. Both compounds exhibit two endothermic peaks upon heating and two

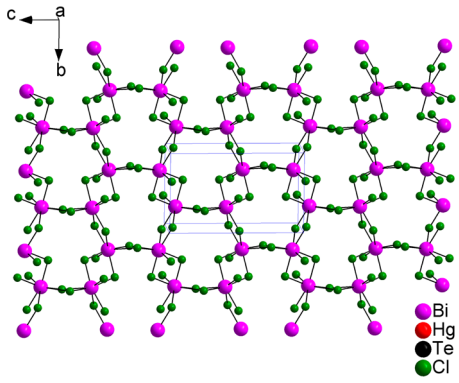

Figure 6. 2D network formation of Bi_2Cl_8 of compound **2** (viewed along the *a* axis), showing the formation of edge-sharing monocapped trigonal prisms. See the text for details.

exothermic peaks upon cooling, which are slightly shifted from cycle 1 to cycle 2 (Figure S4 in the SI). There are two new endothermic peaks (labeled with arrows for clarity), in addition to previous two endothermic peaks (also labeled with arrows), observed upon a second heating for compound **2** (Figure S4b in the SI). The shifting of the original DTA peaks and the appearance of new peaks indicate that the compounds are incongruently melting. This confirms our observations described above regarding the synthetic chemistry of these materials. The PXRD pattern of compound **1** after DTA measurements shows the formation of β-$Hg_3S_2Cl_2$, in addition

dx.doi.org/10.1021/ic3023826 | *Inorg. Chem.* XXXX, XXX, XXX−XXX

to the presence of **1** and BiSCl (Figure S5 in the SI). Similarly, the PXRD pattern after DTA measurements showed the formation of $Hg_3Te_2Cl_2$, which confirms the incongruent melting behavior of compound **2**. In this PXRD pattern, the presence of compound **2**, BiTeCl, and two minute peaks as assigned to BiTe (marked as *) was also observed (Figure S6 in the SI).

Optical Properties. Diffuse-reflectance UV−vis/near-IR (NIR) spectra were collected for both compounds **1** and **2** at room temperature. The room temperature band gap of compound **1** is ∼3.26 eV (Figure 7), in accordance with the white platelike crystals obtained. The spectrum of compound **2** (Figure 8) shows a band gap of 2.80 eV.

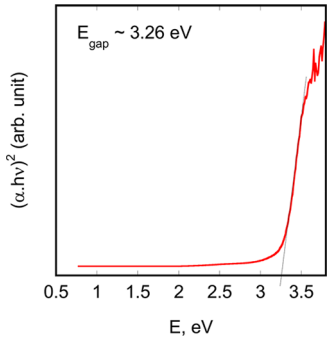

Figure 7. Diffuse-reflectance UV−vis/NIR spectrum of compound **1** measured at room temperature, showing a band gap of 3.26 eV.

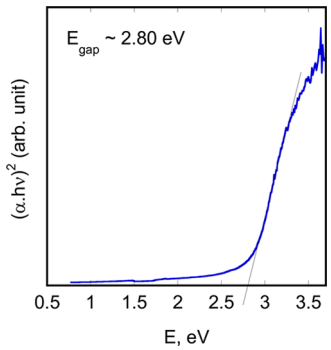

Figure 8. Diffuse-reflectance UV−vis/NIR spectrum of compound **2** measured at room temperature, showing a band gap of 2.80 eV.

Band Structure. To understand the electronic structures of compounds **1** and **2**, we performed the first-principles DFT electronic-structure calculations. We used the experimental lattice constants and atomic structures for these calculations. First, to figure out atomic orbital contributions at band edges, we calculated the projected density of states (PDOS) for both compounds including SOC. As shown in Figure 9a, the valence band maximum (VBM) of compound **1** is mainly composed of the Cl p orbital and a relatively small contribution of the S p orbital, while the conduction band minimum (CBM) consists of Bi p and Cl p orbitals. Without SOC, the CBM are mainly Hg s and S p orbitals (see the inset of Figure 9a); however, a large spin−orbit splitting in Bi p orbitals leads to a change in the atomic orbital contribution at the CBM when we include SOC. In compound **2**, the same situation occurs; the VBM consists of the Cl p orbital and a relatively small contribution of the Te p orbital, and the atomic orbital composition at the CBM is changed from Hg s/Te p orbitals to Bi p/Cl p orbitals

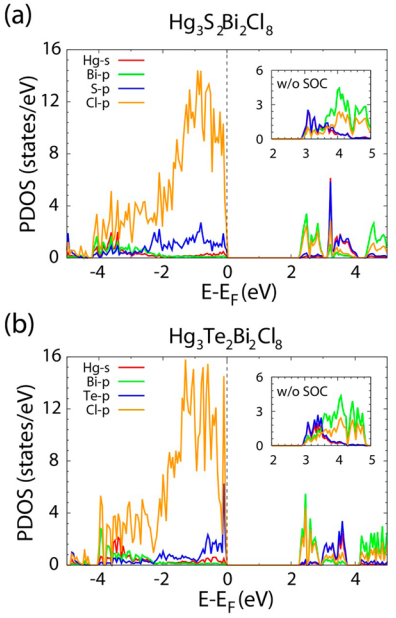

Figure 9. PDOS for **1** (a) and **2** (b) with the LDA including SOC. In both panels, red, green, and orange solid lines correspond to Hg s, Bi p, and Cl p orbital contributions, respectively. The blue solid line means the S p (a) and Te p (b) orbitals. The insets in parts a and b present LDA band structures without SOC near the CBM.

due to SOC, as shown in Figure 9b. Because of the similarity in the electronic structures of both compounds, compounds **1** and **2** have a similar band-gap character, whose VBM is from Cl p orbitals in the Bi−Cl layer and CBM is from Bi p and Cl p orbitals in the Bi−Cl layer.

In order to calculate the band gaps as well as the shape of band edges of the two compounds accurately, we performed sX-LDA band-structure calculations including SOC. As shown in the previous PDOS in Figure 9, the spin−orbit splitting in bismuth orbitals are quite large at the CBM; thus, it significantly affects the band-gap sizes of the two compounds. Furthermore, sX-LDA has shown a great improvement in the excited electronic structure in terms of correctly determining the band gap and band dispersion for wide-range semiconductors. The calculated band structures of compounds **1** and **2** are presented in parts a and b of Figure S7 in the SI, respectively. While LDA calculations yield band gaps of 3.06 eV without SOC and 2.26 eV with SOC in compound **1**, the band-structure calculations using sX-LDA including SOC predicts a band gap of 3.09 eV. In addition, the result from the calculation using sX-LDA with SOC shows that the band topology near the CBM is significantly changed due to a larger spin−orbit splitting in the Bi p orbitals at the Γ point. Moreover, the indirect band gap indicated in the LDA calculation is changed to a direct band gap between the VBM and CBM at Γ in the SOC and sX-LDA+SOC calculations. Compound **2** also follows a similar tendency shown in compound **1**; LDA calculations of compound **2** show an indirect band gap of 2.91 eV without SOC and a direct band gap of 2.28 eV with SOC, while the calculation using sX-LDA with SOC determines an indirect band gap of 2.80 eV.

■ CONCLUSIONS

The quaternary mercury and bismuth chalcohalides $Hg_3Q_2Bi_2Cl_8$ (Q = S, Se, Te) can be synthesized using

dx.doi.org/10.1021/ic3023826 | Inorg. Chem. XXXX, XXX, XXX−XXX

synthetic conditions designed to suppress their tendency for phase separation. The compounds combine two important features needed for good X-ray and γ-ray detection applications, namely, high specific densities, high atomic numbers, and wide energy gaps of 3.26 and 2.80 eV for compounds **1** and **2**, respectively. Because of their incongruent melting nature, however, it will be a challenge to grow large centimeter-sized crystals of these compounds using conventional Bridgman growth technique. Electronic-structure calculation using sX-LDA including SOC shows that SOC of the bismuth atom plays an important role in determining the CBM and predicts that compound **1** has a direct band gap of 3.09 eV, while compound **2** has an indirect band gap of 2.80 eV, in a good agreement with the experimental results.

■ ASSOCIATED CONTENT

Supporting Information

Further details in Table S1 and Figures S1–S7 and X-ray crystallographic data in CIF format. This material is available free of charge via the Internet at http://pubs.acs.org.

■ AUTHOR INFORMATION

Corresponding Author

*E-mail: m-kanatzidis@northwestern.edu.

Notes

The authors declare no competing financial interest.

■ ACKNOWLEDGMENTS

This work was supported by the Office of Nonproliferation and Verification Research and Development under the National Nuclear Security Administration of the U.S. Department of Energy under Contract DE-AC02-06CH11357.

■ REFERENCES

(1) (a) Kabbour, H.; Cario, L. *Inorg. Chem.* **2006**, *45*, 2713–2717. (b) Gunther, A.; Heise, M.; Wagner, F. R.; Ruck, M. *Angew. Chem., Int. Ed.* **2011**, *50*, 9987–9990. (c) Long, J. R.; McCarty, L. S.; Holm, R. H. *J. Am. Chem. Soc.* **1996**, *118*, 4603–4616. (d) Long, J. R.; Williamson, A. S.; Holm, R. H. *Angew. Chem., Int. Ed.* **1995**, *34*, 226–229. (e) Sokolov, M. N.; Gushchin, A. L.; Abramov, P. A.; Virovets, A. V.; Peresypkina, E. V.; Fedin, V. P. *Inorg. Chem.* **2007**, *46*, 4677–4682. (f) Gabriel, J.-C. P.; Boubekeur, K.; Uriel, S.; Batail, P. *Chem. Rev.* **2001**, *101*, 2037–2066 and references cited therein. (g) Smith, M. D.; Miller, G. J. *J. Am. Chem. Soc.* **1996**, *118*, 12238–12239. (h) Pfitzner, A.; Reiser, S.; Nilges, T. *Angew. Chem., Int. Ed.* **2000**, *39*, 4160–4162. (i) Beck, J.; Dolg, M.; Schluter, S. *Angew. Chem., Int. Ed.* **2001**, *40*, 2287–2290. (j) Biswas, K.; Zhang, Q.; Chung, I.; Song, J.-H.; Androulakis, J.; Freeman, A. J.; Kanatzidis, M. G. *J. Am. Chem. Soc.* **2010**, *132*, 14760–14762. (k) Deiseroth, H.-J.; Kong, S.-T.; Eckert, H.; Vannahme, J.; Reiner, C.; Zaib, T.; Schlosser, M. *Angew. Chem., Int. Ed.* **2008**, *47*, 755–758.

(2) (a) Androulakis, J.; Peter, S. C.; Li, H.; Malliakas, C. D.; Peters, J. A.; Liu, Z.; Wessels, B. W.; Song, J.-H.; Jin, H.; Freeman, A. J.; Kanatzidis, M. G. *Adv. Mater.* **2011**, *23*, 4163–4167. (b) Johnsen, S.; Liu, Z.; Peters, J. A.; Song, J.-H.; Nguyen, S.; Malliakas, C. D.; Jin, H.; Freeman, A. J.; Wessels, B. W.; Kanatzidis, M. G. *J. Am. Chem. Soc.* **2012**, *133*, 10030–10033. (c) Malliakas, C. D.; Wibowo, A. C.; Liu, Z.; Peters, J. A.; Sebastian, M.; Jin, H.; Chung, D.-Y.; Freeman, A. J.; Wessels, B. W.; Kanatzidis, M. G. *Proc. SPIE* **2012**, *8507*, 14.

(3) (a) Guo, S.-P.; Guo, G.-C.; Wang, M.-S.; Zou, J.-P.; Zeng, H.-Y.; Cai, L.-Z.; Huang, J.-S. *Chem. Commun.* **2009**, 4366–4368. (b) Zhang, Q.; Chung, I.; Jang, J. I.; Ketterson, J. B.; Kanatzidis, M. G. *J. Am. Chem. Soc.* **2009**, *131*, 9896–9897. (c) Cai, Y.; Wang, Y.; Li, Y.; Wang, X.; Xin, X.; Liu, C.; Zheng, H. *Inorg. Chem.* **2005**, *44*, 9128–9130.

(4) (a) Nilges, T.; Osters, O.; Bawohl, M.; Bobet, J.-L.; Chevalier, B.; Decourt, R.; Weihrich, R. *Chem. Mater.* **2010**, *22*, 2946–2954. (b) Kong, S.-T.; Deiseroth, H.-J.; Reiner, C.; Gun, O.; Neumann, E.; Ritter, C.; Zahn, D. *Chem.—Eur. J.* **2010**, *16*, 2198–2206. (c) Gagor, A.; Pietraszko, A.; Kaynts, D. *J. Solid State Chem.* **2005**, *178*, 3366–3375.

(5) (a) Xu, Y.; Chen, D.; Zhang, Q.; Zeng, H.; Shen, C.; Adam, J.-l.; Zhang, X.; Chen, G. *J. Phys. Chem. C* **2009**, *113*, 9911–9915. (b) Wang, W.; Zhang, Q.; Xu, Y.; Shen, C.; Chen, D.; Chen, G. *J. Am. Ceram. Soc.* **2010**, *93*, 2445–2447.

(6) (a) Morsali, A.; Masoomi, M. Y. *Coord. Chem. Rev.* **2009**, *253*, 1882–1905. (b) Wibowo, A. C.; Smith, M. D.; Loye, H.-C. z. *Chem. Commun.* **2011**, *47*, 7371–7373. (c) Wibowo, A. C.; Smith, M. D.; Loye, H.-C. z. *CrystEngComm* **2011**, *13*, 426–429. (d) Wibowo, A. C.; Vaughn, S. A.; Smith, M. D.; Loye, H.-C. z. *Inorg. Chem.* **2010**, *49*, 11001–11008. (e) Wibowo, A. C.; Smith, M. D.; Loye, H.-C. z. *Cryst. Growth Des.* **2011**, *11*, 4449–4457. (f) Stavila, V.; Davidovich, R. L.; Gulea, A.; Whitmire, K. H. *Coord. Chem. Rev.* **2006**, *250*, 2782–2810 and references cited therein.

(7) Bugaris, D. E.; Ibers, J. A. *J. Solid State Chem.* **2008**, *181*, 3189–3193.

(8) Beck, J.; Hedderich, S. *J. Solid State Chem.* **2003**, *172*, 12–16.

(9) Beck, J.; Hedderich, S.; Kollisch, K. *Inorg. Chem.* **2000**, *39*, 5847–5850.

(10) Chen, W.-T.; Kuang, H.-M.; Chen, H.-L. *J. Solid State Chem.* **2010**, *183*, 2411–2415.

(11) Jiang, X.-M.; Zhang, M.-J.; Zeng, H.-Y.; Guo, G.-C.; Huang, J.-S. *J. Am. Chem. Soc.* **2011**, *133*, 3410–3418.

(12) Zou, J.-P.; Peng, Q.; Luo, S.-L.; Tang, X.-H.; Zhang, A.-Q.; Zeng, G.-S.; Guo, G.-C. *CrystEngComm* **2011**, *13*, 3862–3867.

(13) Liu, Y.; Wei, F.; Yeo, S. N.; Lee, F. M.; Kloc, C.; Yan, Q.; Hng, H. H.; Ma, J.; Zhang, Q. *Inorg. Chem.* **2012**, *51*, 4414–4416.

(14) (a) Morris, C. D.; Kanatzidis, M. G. *Inorg. Chem.* **2010**, *49*, 9049–9054. (b) Liao, J. H.; Marking, G. M.; Hsu, K. F.; Matsushita, Y.; Ewbank, M. D.; Borwick, R.; Cunningham, P.; Rosker, M. J.; Kanatzidis, M. G. *J. Am. Chem. Soc.* **2003**, *125*, 9484–9493. (c) Larson, P.; Mahanti, S. D.; Kanatzidis, M. G. *Phys. Rev. B* **2000**, *61*, 8162. (d) McCarthy, T. J.; Tanzer, T. A.; Kanatzidis, M. G. *J. Am. Chem. Soc.* **1995**, *117*, 1294. (e) Trikalitis, P. N.; Rangan, K. K.; Bakas, T.; Kanatzidis, M. G. *J. Am. Chem. Soc.* **2002**, *124*, 12255.

(15) Wimmer, E.; Krakauer, H.; Weinert, M.; Freeman, A. J. *Phys. Rev. B* **1981**, *24*, 864–875.

(16) Hedin, L.; Lundqvist, B. I. *J. Phys. C: Solid State Phys.* **1971**, *4*, 2064–2083.

(17) McDonald, A. H.; Pickette, W. E.; Koeling, D. D. *J. Phys. C: Solid State Phys.* **1980**, *13*, 2675–2683.

(18) Bylander, D. M.; Kleinman, L. *Phys. Rev. B* **1990**, *41*, 7868–7871.

(19) Kim, M.; Freeman, A. J.; Geller, C. B. *Phys. Rev. B* **2005**, *72*, 035205.

dx.doi.org/10.1021/ic3023826 | *Inorg. Chem.* XXXX, XXX, XXX–XXX